

Brownian ratchet driven by Coulomb friction

Andrea Gnoli

*Istituto dei Sistemi Complessi - CNR, via del Fosso del Cavaliere 100, 00133 Rome, Italy and
Istituto dei Sistemi Complessi - CNR and Dipartimento di Fisica,
Università "Sapienza", p.le A. Moro 2, 00185 Rome, Italy*

Alberto Petri, Fergal Dalton, and Giorgio Pontuale

Istituto dei Sistemi Complessi - CNR, via del Fosso del Cavaliere 100, 00133 Rome, Italy

Giacomo Gradenigo, Alessandro Sarracino, and Andrea Puglisi

*Istituto dei Sistemi Complessi - CNR and Dipartimento di Fisica,
Università "Sapienza", p.le A. Moro 2, 00185 Rome, Italy*

The rectification of unbiased fluctuations, also known as ratchet effect, can be obtained under statistical non-equilibrium conditions. Recently, it has been demonstrated that it is possible to rectify the fluctuations of macroscopic mechanical devices, for instance, by suspending an asymmetric probe in a fluidized granular medium. Here we demonstrate experimentally the existence of a ratchet effect entirely originated from the Coulomb friction. Such a friction-induced torque acts in the opposite direction with respect to the net torque provided by inelastic collisions between the ratchet and the granular fluid, resulting in a resonant behaviour and a ratchet velocity inversion point. Our experimental observations are reproduced by simulations and explained by kinetic theory. Our discovery paves the way to the realization of Brownian motors in the realm of micro and sub-micrometer scales purely based upon nano-friction.

PACS numbers: 02.50.Ey, 05.20.Dd, 81.05.Rm

From microscopic organisms to muscle fibres, from electric motors to power stations, the biosphere, our society and our lives critically depend on the conversion of energy to mechanical work. Thermodynamics provides precise and well established rules for energy conversion in macroscopic systems but these rules become blurred at small scales when thermal fluctuations play a decisive role [1]. Extracting work under such conditions requires subtle strategies radically different from those effective in the macroscopic world [2–7]. Within this framework, the theory of Brownian motors deals with the rectification of thermal fluctuations, a goal which can only be achieved in the presence of dissipation [8–13]. An interesting class of systems, where both dissipation and fluctuations are relevant, is represented by granular media [14, 15]. Indeed, interactions in a granular system are inherently dissipative, and because of its small number of constituents when compared with molecular gases or liquids, a granular fluid presents large fluctuations. The additional break of spatial symmetry is sufficient for a motor effect to be generated as demonstrated in a series of experiments [16–18] and theoretical works [19–24].

In previous works the main source of dissipation was provided by the inelasticity of collisions, a property normally not present at micro or nanometric scales. The remarkable result of our study is the discovery of an unexpectedly efficient source of dissipation that contributes to rectify unbiased fluctuations: the Coulomb (also called “dry”) friction [25, 26]. We show that the irreversibility generated by the dry friction works also in the case of fully elastic collisions and can therefore be exploited

in micro and nano apparatuses where friction is still present [27, 28].

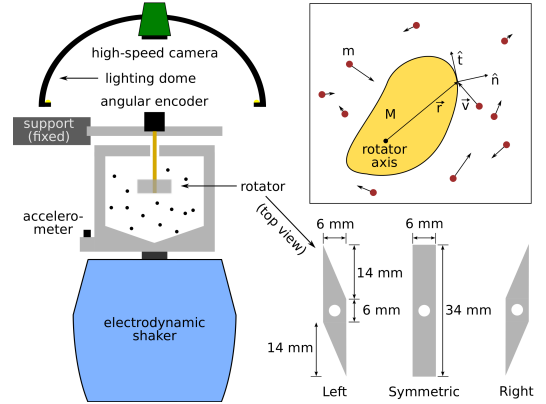


FIG. 1: Experimental set-up. The asymmetric rotator is shown in its “left” and “right” configurations. The inset shows the definition of quantities used in the text for a generic-shaped rotator.

In our experiment we observe the angular motion of a rotator vertically suspended in a fluidized granular medium (see Figure 1) [15, 29]. The granular medium is contained in a volume V and is composed of N spheres of mass m and radius r and is maintained by an electrodynamic shaker in a stationary gaseous regime, roughly homogeneous at an average number density $n = N/V$. The shaker performs a vertical sinusoidal oscillation at a frequency of 53 Hz, while the amplitude is varied to

explore different regimes of the system. The motion of the rotator is recorded by an angular encoder which also provides its support. We use two rotators of different shape, mass M and momentum of inertia I : the first being symmetric with respect to its direction of rotation, the second having an asymmetric ratchet shape as shown in Figure 1. The asymmetry of the latter can be inverted (from left to right hand, and vice versa) simply by turning the rotator upside-down. As much as the rotator is constrained to rotate about its axis during experiments, only the 2D *chiral* profile is relevant in our analysis and hence we also refer to the asymmetric rotators as chiral.

The angular velocity of the rotator $\omega(t)$ is affected by collisions with the granular medium, by the viscous drag $-\Gamma_{visc}\omega$ due to the surrounding air and by Coulomb friction torque $-F_{friction}\sigma(\omega)$ (where $\sigma(x)$ is the sign function) due to the bearings in the support, resulting in

$$\dot{\omega}(t) = -\gamma_a\omega(t) - \sigma[\omega(t)]\Delta + \eta_{coll}(t) \quad (1)$$

where $\gamma_a = \Gamma_{visc}/I$, $\Delta = F_{friction}/I$ and $\eta_{coll}(t)$ is the noise due to collisions with the grains. To characterize the “granular bath” surrounding the rotator, we have measured - using a high-speed camera - the spheres’ speed projected on the rotation plane in order to determine the “thermal” velocity $v_0 = \sqrt{\langle v^2 \rangle}$ of the granular gas, where v is v_x or v_y (isotropy has been verified). The amplitude of the shaker oscillation is varied to span a range of maximum acceleration (in units of gravity acceleration) between 5 to 20, resulting in a granular thermal velocity v_0 ranging between ~ 100 mm/s and ~ 600 mm/s. Details on the experimental setup and measurement of the parameters can be found in the Supplemental Material [30].

In Figure 2, we provide some runs demonstrating the ratchet effect for the chiral rotator. A net drift is evident when a chiral rotator is used. Reversing the chirality results in a reversed direction of rotation. The symmetric rotator makes a diffusive motion with only a small drift revealing the presence of some bias due to imperfections in the rotational symmetry of the setup. Such a bias affects also the curves pertaining to the chiral rotator and it does not appear to depend on the rotator’s direction of asymmetry, or absence thereof. The typical instantaneous velocity of rotators is $\sim 10^{-1} \div 1$ rad/s, much larger than the typical ratchet drift $\sim 10^{-4} \div 10^{-2}$ rad/s. Such a low signal-to-noise ratio makes it impossible to determine the true behaviour of the rotator if one monitors its position only for short times (e.g. less than a few hours), as evidenced in the inset of Figure 2.

For the purpose of a systematic investigation, it is useful to realize that two time-scales are relevant in the system: 1) the mean stopping time due to environmental dissipation, which is dominated by dry friction (being almost always $\gamma_a|\omega| < \Delta$), $\tau_\Delta = \frac{\langle |\omega| \rangle_{pc}}{\Delta} \sim \frac{\epsilon v_0}{R_I \Delta}$, where $\langle \cdot \rangle_{pc}$ denotes a post-collisional average, $R_I = \sqrt{I/M}$ is the radius of inertia and $\epsilon = \sqrt{m/M}$; 2) the mean free

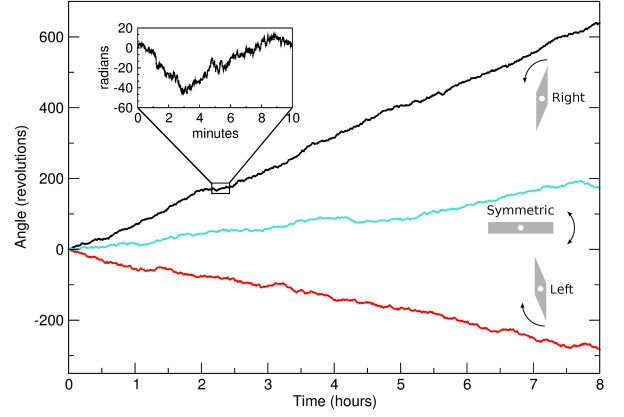


FIG. 2: The angular position of the rotator as a function of time, highlighting the ratchet effect for the chiral rotator. The inset shows an enlargement (ten minutes) extracted from a chiral (right) experiment. For these experiments the value of maximum acceleration, normalized by gravity, is 13.

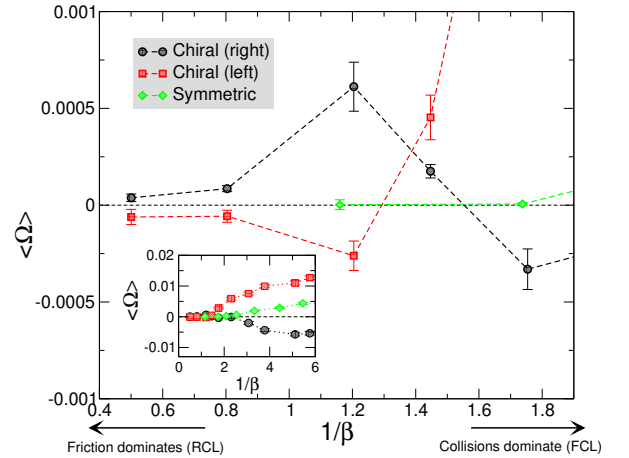


FIG. 3: Plot of the rescaled angular velocity of the rotator, $\langle \Omega \rangle = \frac{R_I}{\epsilon v_0} \langle \omega \rangle$, averaged on an 8-hours run, as a function of β^{-1} which estimates the ratio of time-scales $\frac{\tau_\Delta}{\tau_c}$. The main plot shows the region where a maximum and a current inversion are observed for the chiral rotator. The inset sums all the results up, highlighting the behaviour for small β^{-1} . Experiments are performed with maximum shaker acceleration varying in the range of $5 \div 20$ in gravity units.

time between two collisions $\tau_c \sim \frac{1}{n\Sigma v_0}$ where Σ is the surface (parallel to the rotation axis) of the rotator. We therefore use as main control parameter

$$\beta^{-1} = \frac{\epsilon n \Sigma v_0^2}{\sqrt{2\pi} R_I \Delta} \approx \frac{\tau_\Delta}{\tau_c} \quad (2)$$

which is an estimate of the ratio of those two time-scales, as verified by simulations (see below).

In Figure 3, we show the average adimensional angular velocity $\langle\Omega\rangle = \frac{R_L}{\epsilon v_0}\langle\omega\rangle$ for a set of experiments with chiral and symmetric rotators. The behaviour with β^{-1} displays several interesting phenomena. At $\beta^{-1} < 1$, we measure $|\langle\Omega\rangle|$ increasing with β^{-1} , followed by a maximum in the proximity of $\beta^{-1} \sim 1$ and then by an inversion of direction of motion. At large β^{-1} , $|\langle\Omega\rangle|$ increases and finally reaches a plateau (see inset of Figure 3).

An account for such a complex behaviour can be obtained through kinetic theory, by assuming Molecular Chaos (the packing fraction of our gas is lower than 3%). The probability density function (pdf) $p(\omega, t)$ for the angular velocity is therefore fully described by the following linear Boltzmann equation [22, 24]

$$\partial_t p(\omega, t) = \partial_\omega [(\Delta\sigma(\omega) + \gamma_a\omega)p(\omega, t)] + J[p, \phi] \quad (3a)$$

$$J[p, \phi] = \int d\omega' W(\omega|\omega')p(\omega', t) - p(\omega, t)f_c(\omega), \quad (3b)$$

where we introduce the rate $W(\omega'|\omega)$ for the transition $\omega \rightarrow \omega'$ and the velocity-dependent collision frequency $f_c(\omega) = \int d\omega' W(\omega'|\omega)$. The rate $W(\omega'|\omega)$, given explicitly in the Supplemental Material [30], depends on the velocity distribution of the gas particles, on the restitution coefficient α , on the rotator cross section and on the density of the gas.

The above equation is simplified in the two following opposite limits [22, 24]: when $\beta^{-1} \gg 1$ ($\tau_c \ll \tau_\Delta$) the dynamics of the rotator is dominated by collisions and friction is negligible (frequent collisions limit, FCL); in the opposite limit $\beta^{-1} \ll 1$ ($\tau_c \gg \tau_\Delta$, rare collisions limit, RCL) the rotator remains most of the time at rest and is rarely perturbed by collisions acting as independent random excitations.

When the mass of the rotator is large, $\epsilon \ll 1$ (in our experiment $\epsilon = 0.15$) the FCL is perturbatively reduced to a Brownian approximation and the average drift can be computed giving [24]

$$\langle\Omega\rangle = \epsilon \sqrt{\frac{\pi}{2}} \frac{1-\alpha}{4} \mathcal{A}_{FCL} \quad (4a)$$

$$\mathcal{A}_{FCL} = -\frac{\langle g^3 \rangle_{surf}}{\langle g^2 \rangle_{surf}}, \quad (4b)$$

where the asymmetry of the rotator is represented by \mathcal{A}_{FCL} which is 0 for a symmetric (non-chiral) rotator; above we have used the shorthand notation for the uniform average along the perimeter (denoted as “surface”) of a horizontal section of the rotator $\langle \rangle_{surf} = \int_{surf} \frac{ds}{S}$ (S being the total perimeter, see Supplemental Material [30]), while $g = \frac{r_L}{R_L}$; see Figure 1 for an explanation of symbols. This formula predicts zero net drift either with elastic collisions ($\alpha = 1$) or with a symmetric rotator ($\mathcal{A}_{FCL} = 0$), as expected by symmetry arguments. Most importantly, it predicts a constant value for the chiral case, as verified in the experiment, which means $|\langle\omega\rangle| \sim v_0$ for the *dimensional* angular velocity.

The study of the RCL leads to remarkably different predictions. In such a limit, the dynamics after each collision event produces an increment of the angular position of the rotator $\Delta\theta$ which depends on the velocity \mathbf{v} of the gas particle, precisely on its projection $v = \mathbf{v} \cdot \hat{n}$, and on the point of impact represented for instance by its curvilinear abscissa s . The formula is $\Delta\theta(v, s) = \sigma(\omega_0) \frac{\omega_0^2}{2\Delta}$ with $\omega_0 = -(1+\alpha) \frac{v}{R_L} \frac{\epsilon^2 g}{1+\epsilon^2 g^2}$. Following the calculations detailed in Supplemental Material [30], one obtains the formula for the rescaled average velocity of the ratchet

$$\langle\Omega\rangle = \sqrt{\pi}(1+\alpha)^2 \beta^{-1} \epsilon^2 \mathcal{A}_{RCL} \quad (5a)$$

$$\mathcal{A}_{RCL} = \left\langle \frac{\sigma(g)g^2}{(1+\epsilon^2 g^2)^2} \right\rangle_{surf}, \quad (5b)$$

where $\mathcal{A}_{RCL} = 0$ for symmetric (i.e. non-chiral) shapes of the rotator. The above formula shows that a non-zero drift is achieved *independently* of the elasticity of the rotator: even in the (ideal) elastic case, Coulomb friction alone produces the desired ratchet effect provided that the shape of the rotator is not symmetric, i.e. that $\mathcal{A}_{RCL} \neq 0$. Note that the limit $\Delta \rightarrow 0$ is singular in formula (5a), since in the absence of dissipation between collisions the stopping time becomes infinite, $\tau_\Delta \rightarrow \infty$, and the assumption of “rare collisions” breaks down. Equally interesting, the shape factor \mathcal{A}_{RCL} , determining the intensity and drift direction in the RCL, can take *opposite sign* with respect to the shape factor \mathcal{A}_{FCL} in the FCL formula. This is precisely the case of the chosen shape, see Fig. 1. Moreover, the magnitude of the drift is predicted to increase with β^{-1} as seen in the experiment for small β^{-1} . This corresponds to $|\langle\omega\rangle| \sim v_0^3$.

For an insight into theory, we performed Direct Simulation Monte Carlo [34] simulations (see Supplemental Material [30] for details) whose results are summarized in Fig. 4. As expected from the above analytical formula and consistently with the experiments, the drift of the chiral rotator is non-vanishing even in the elastic case for small β^{-1} . In the inelastic case $\alpha < 1$, it takes different signs in the two limits, FCL and RCL, requiring the existence of at least one inversion point; moreover, the behaviour in the RCL ($|\langle\Omega\rangle|$ growing with $\frac{\tau_\Delta}{\tau_c}$) requires that the inversion point is reached by going through (at least) a maximum, which is indeed observed at $\tau_\Delta \sim \tau_c$, as in the experiments. Such a maximum, observed also in the elastic case, can be viewed as a kind of *stochastic resonance*: the rotator switches from the “drift” state to the “rest” state on the time-scale τ_Δ and switches back to the “drift” state on the time-scale τ_c ; when the two scales synchronize with each other, the total time spent in the “drift” state is maximized, as well as its average velocity. We note that current inversion in Brownian motors has been already observed [31–33].

A comment is needed for the quantitative comparison between theory (or simulation) and the experiments, whereas on the qualitative side the agreement is more

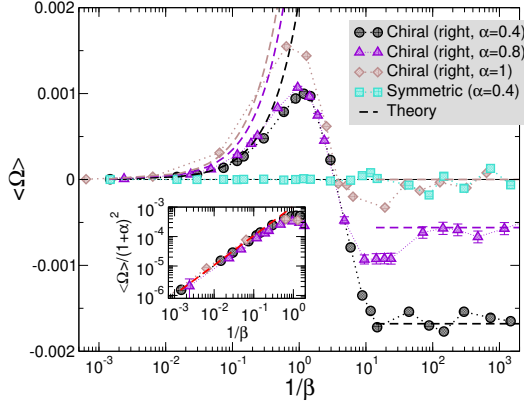


FIG. 4: Simulations. The dynamics of the rotator, consisting of relaxations under the effect of dissipations (dry and viscous friction) plus excitation due to collisions, is simulated under the assumption of Molecular Chaos. The rescaled average angular velocity $\langle \Omega \rangle$ is shown as a function of β^{-1} . Theoretical expectations in the FCL and RCL are marked by dashed lines. The inset zooms in the RCL region. Simulations are performed using the experimental shapes, $R_I/\epsilon = 10^3$ and $v_0 = 100$ in arbitrary units (varying $n\Sigma$ to obtain a variation of β^{-1}).

than satisfying. The simulations, done in conditions similar to the experiment, show the local maximum of $|\langle \Omega \rangle|$ near $\beta^{-1} \sim 1$ to be of the order of 10^{-3} , not far from that 0.5×10^{-3} experimentally measured. The FCL plateau for $|\langle \Omega \rangle|$ found in the experiment is though ~ 5 times larger than the theoretical one. In connection with this point, however, the following consideration applies: the theoretical model is based on many assumptions, the most important being molecular chaos and spatial homogeneity, which can be hardly controlled in the experiment. Thus, we suspect that a stronger drift can be ascribed to non-equilibrium correlations (in the density and also in the velocity distribution) which become important at high collision frequencies [35].

To conclude, our experimental observations, supported by numerical simulations and kinetic theory, neatly point to Coulomb friction as a relevant mechanism for exploiting the ratchet effect. Even though it is obviously impossible to realize perfectly elastic collisions in macroscopic systems, our findings indicate that extraction of work can be achieved and controlled at the micro- and nano-scopic scale, where perfectly elastic interactions and friction can coexist.

We would like to thank A. Vulpiani for useful comments and MD. Deen for technical support. The authors acknowledge the support of the Italian MIUR under the grants: FIRB-IDEAS number RBID08Z9JE, and FIRB number RBFR081IUK.

SUPPLEMENTAL MATERIAL

Experimental set-up.

Our model assumes that the evolution of the angular velocity ω of the rotator obeys an equation of the form

$$I\dot{\omega}(t) = -F_{friction}\sigma[\omega(t)] - \Gamma_{visc}\omega(t) + F_{coll}(t), \quad (6)$$

where I is the momentum of inertia, $F_{friction}$ is the dry friction torque, σ the sign function and Γ_{visc} the air viscous drag. The term $F_{coll} = I\eta_{coll}$ contains the driving torque, that is the angular momentum randomly transferred from the beads to the rotator, and is analysed in detail in Section 2. We refer to Figure 1 of the paper for the main features of our set-up. Dissipation coefficients rescaled by inertia are $\gamma_a = \Gamma_{visc}/I$ and $\Delta = F_{friction}/I$.

Technical details about the experimental setup. The granular medium, made of 50 polyoxymethylene (POM) spheres (radius $r = 3$ mm and mass $m = 0.15$ g), is housed in a polymethyl-methacrylate (PMMA) cylinder (diameter 90 mm) with a conical-shaped floor. A removable cap encloses a miniaturized angular encoder (model AEDA-3300 by Avago Technologies). The encoder, which also supports the rotator, provides high resolution measurements (up to 80,000 division/revolution at the maximum rate of 20 kHz) of the rotator position. The system is vibrated by an electrodynamic shaker (model V450 by LDS Test & Measurement) fed by a sinusoidal excitation. An accelerometer measures the actual acceleration induced to the system. A high-speed camera (EoSens CL by Mikrotron) tracks single beads in order to measure their velocity. The two rotators are made of PMMA, have height $h = 15$ mm and are distinguished by their different section on the rotation plane. The momentum of inertia of the rotator I comprises different parts. The probe is attached to the angular encoder by means of a steel rotation axis 50 mm high and 3 mm thick. The mass of the whole rotator (axis and probe) is $M = 5.21$ g for the asymmetric probe and $M = 6.49$ g for the symmetric one. The total momentum of inertia is $I = 135$ gmm² and $I = 353$ gmm² for the two types, respectively. In both cases the inertia of the axis is a few hundredths of the total one. The shape factors of the asymmetric rotator, relevant for its ratchet effect, are $\left\langle \frac{\sigma(g)g^2}{(1+\epsilon^2g^2)} \right\rangle_{surf} = 0.0013$ and $\frac{\langle g^3 \rangle_{surf}}{\langle g^2 \rangle_{surf}} = 0.052$ for the RCL and FCL limits respectively (see text for definitions). Both the shape factors vanish for the symmetric rotator.

Dry and viscous friction. The only source of dry friction comes from the two ball bearings inside the encoder while viscous friction is due to the air surrounding the rotator. We measure the dry and viscous friction during a standard experimental run (eight hours), but considering only periods where the rotator is subject to these forces and no other: $\dot{\omega} = -\gamma_a\omega \mp \Delta$ (where the upper sign holds

for $\omega > 0$ and the lower for $\omega < 0$), i.e. excluding the time immediately about collisions and periods of rest. Angular velocity and acceleration are obtained from the angular position (in function of time) by differentiation. A bidimensional histogram is calculated and a peak-finding procedure has been applied in order to obtain the most probable trajectories in $(\omega, \dot{\omega})$ space. Finally, the most probable trajectory is fitted with the above linear equations, yielding the values $F_{friction} = (9.9 \pm 0.7) \times 10^3 \text{ g mm}^2/\text{s}^2$ and $\Gamma_{visc} = (1.6 \pm 0.2) \times 10^3 \text{ g mm}^2/\text{s}$. It is interesting to notice that viscous friction becomes important for velocities larger than the threshold velocity $\omega_{th} = F_{friction}/\Gamma_{visc} \approx 6.2 \text{ s}^{-1}$, separating the friction-dominated regime $\omega \ll \omega_{th}$ from the viscosity-dominated one $\omega \gg \omega_{th}$.

Restitution coefficients. The beads-rotator restitution coefficient α has been measured launching a single bead against the rotator while recording the rotator position at high sampling rate (1 kHz). For these measurements the top of the apparatus is removed and put with the rotation axis parallel to the floor. A bead falls from height h and hits the rotator with velocity $v = \sqrt{2a_g h}$ (here a_g indicates the gravity acceleration). The high-speed camera has been used to monitor the exact distance x of the impact point from the rotation axis. We calculate the restitution coefficient using the collision rule (see Section 2 below) adapted for this particular configuration in which the rotator is at rest before the collision ($\Omega = V = 0$) and $g \approx x/R_I$. In this circumstances the velocity of the rotator after a collision is $\omega' = (1 + \alpha)vx/(I/m + x^2)$. Repeated measurements on the symmetric rotator gave the following results: $\alpha = 0.83 \pm 0.16$ (we recall that $\alpha = 1$ for elastic collisions).

Granular gas velocity statistics. We discuss here the methods used to characterize the velocity statistics of the granular gas. A fast camera (EoSens CL by Mikrotrotron) is placed above the PMMA container to catch horizontal components of motion (v_x, v_y) of the polyoxymethylene (POM) spheres constituting the granular gas. Focus of lens is adjusted to the plane at half height of the probe. Lighting is provided by a led-dome which diffuses light on the system reducing shadows and reflections. Particle tracking is enhanced by marking a few tracers: 3 POM spheres are white, while all the other particles are black. Pictures are taken at 250 frames per second: this is verified to be the optimal compromise between too large delays, which prevent tracking of ballistic trajectories, and too small ones, which produce “false movement” induced by noise due to finite sensitivity of the camera resolution and the centring algorithm. Uncertainty in the determination of the centre of mass of tracer spheres is estimated to be $\sim 0.05 \text{ mm}$. The details of velocity measurements and error estimates are reported in [36]. In Figure 5 we display a typical snapshot of the system from the camera (see also the accompanying Movie).

For each choice of shaking parameters we have com-

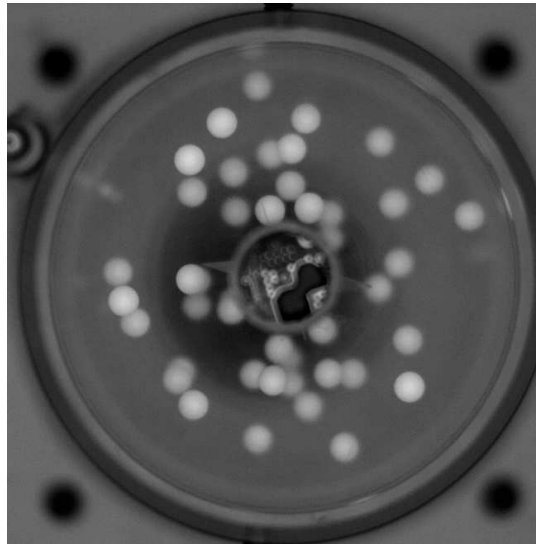


FIG. 5: A snapshot of the system taken from the fast camera (shaker is vibrating at 53 Hz with rescaled maximum acceleration $\Gamma = 8$).

puted the velocity histogram from a series of 2×10^4 contiguous frames. Examples of those histograms are reported in Figure 6, left frame. A Gaussian fit is seen to be a good approximation and provides the value of $v_0 = \sqrt{\langle v^2 \rangle}$ where v is v_x or v_y (isotropy is always verified). In the right frame of Figure 6 we report the values of v_0 as function of the rescaled maximum acceleration $\Gamma = \frac{a_{max}}{a_g}$ where a_g is gravity acceleration and the $z_s(t)$ position of the shaker’s vibrating head follows the law $z_s(t) = \frac{a_{max}}{(2\pi f)^2} \sin(2\pi f t)$ with f being the vibration frequency.

Rotator velocity signal. An example of the velocity signal $\omega(t)$ in two different regimes (frequent and rare collisions) is shown in Figure 7, left frame, for the case of the symmetric rotator. In the right frame of the same Figure, we show the angular velocity autocorrelation $C(t) = \langle \omega(t)\omega(0) \rangle - \langle \omega \rangle^2$ versus time. Note that the signal average is much smaller than its standard deviations and, hence, it is negligible in $C(t)$.

Here, it is interesting to comment about the smaller characteristic time associated to the system with rare collisions (red curve), with respect to that with frequent collisions (black curve): this is a consequence of the smaller typical velocity in the rare collisions configuration, which induces faster relaxations through Coulomb friction dissipation (we recall that $\tau_\Delta \approx \frac{\langle |\omega| \rangle}{\Delta}$). Similar results are obtained with the asymmetric rotator.

Details of the theory

We model our experiment as follows (refer to Figure 1 for a visual explanation of symbols). A rigid body of mo-

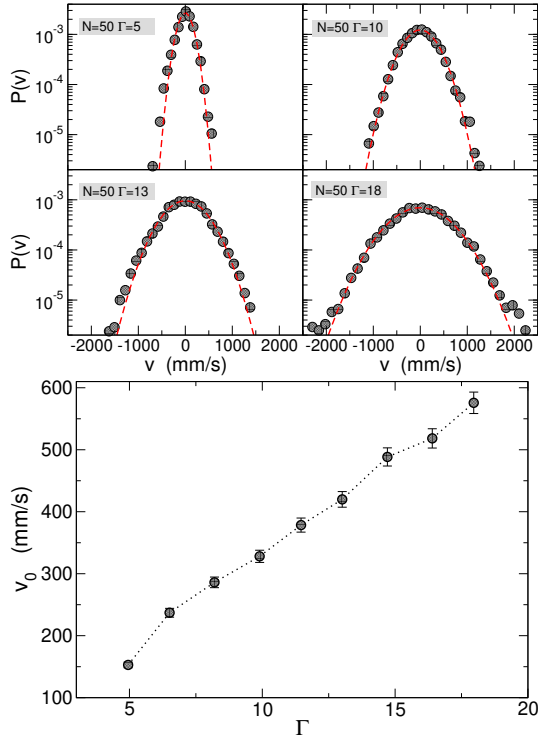


FIG. 6: Left: Histograms of velocities (v_x) of $N = 50$ granular gas particles for different values of the rescaled maximum acceleration Γ at vibration frequency 53 Hz. Gaussian fits are superimposed. Right: the values of v_0 (standard deviation) versus Γ .

momentum of inertia I and total mass M is bound to rotate around a fixed axis (say \hat{z}) and is suspended in a dilute isotropic granular fluid. The body is constituted by the set of material points with cartesian coordinates $\{x, y, z\}$ with $z \in [0, h]$ (where h is the height of the cylinder) and $\sqrt{x^2 + y^2} < r(s)$ for each $s \in [0, S]$ where s is the curvilinear abscissa, $r(s)$ is the curve delimiting a section of the solid in the xy plane, and S is the perimeter of the section. The dilute granular fluid has volume number density n and is made of identical spheres of mass m . We denote by ω the angular velocity of the rotator, by θ its angular position, and by \mathbf{v} the velocity of a granular sphere. We also denote by $\rho = nh$ the two-dimensional projection of density, which is the only one which matters in our problem. Note that $\rho S \equiv n\Sigma$ (as in the Letter) is the total surface of the rotator parallel to the rotation axis.

Inelastic collisions The spheres interact with the rotator by means of inelastic hard-core collisions, which change instantaneously the velocity of the rotator from ω to ω' and that of the colliding particle from \mathbf{v} to \mathbf{v}' ,

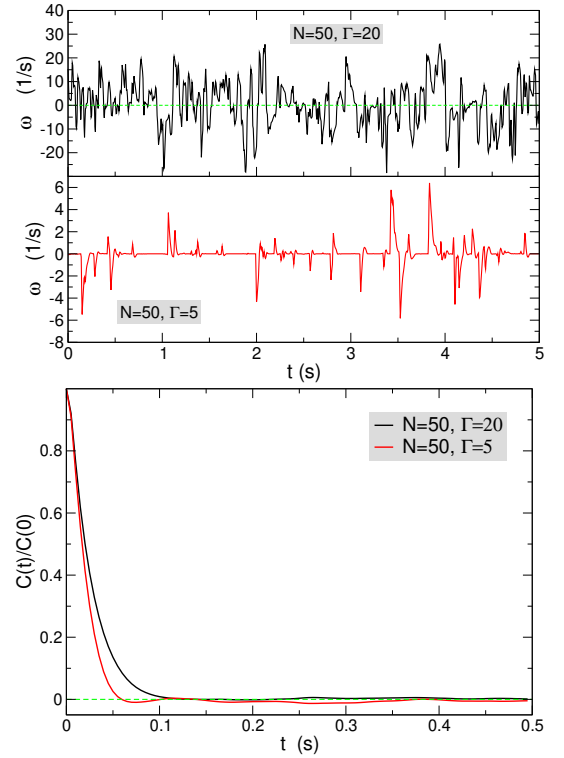


FIG. 7: Left: Examples of symmetrical rotator's angular velocity signal $\omega(t)$ as acquired from the angular encoder at 200 Hz in two different regimes (frequent collisions, top, and rare collisions, bottom). Right: rescaled angular velocity autocorrelation $C(t)/C(0)$ versus time t for the two cases shown in the left frame.

following the rule

$$\omega' = \omega + (1 + \alpha) \frac{(\mathbf{V} - \mathbf{v}) \cdot \hat{n}}{R_I} \frac{g\epsilon^2}{1 + \epsilon^2 g^2}, \quad (7a)$$

$$\mathbf{v}' = \mathbf{v} + (1 + \alpha) \frac{(\mathbf{V} - \mathbf{v}) \cdot \hat{n}}{1 + \epsilon^2 g^2} \hat{n} \quad (7b)$$

where $\alpha \in [0, 1]$ is the restitution coefficient ($\alpha = 1$ corresponds to elastic collisions), $\mathbf{V} = \omega \hat{z} \times \mathbf{r}$ is the linear velocity of the rotator at the point of impact \mathbf{r} , \hat{n} is the unit vector perpendicular to the surface at that point, and finally $g = \frac{\mathbf{r} \cdot \hat{t}}{R_I}$ with $\hat{t} = \hat{z} \times \hat{n}$ which is the unit vector tangent to the surface at the point of impact.

Equations (7) guarantee that total angular momentum $L\hat{z} = m\mathbf{r} \times \mathbf{v} + I\omega\hat{z}$ is conserved, that relative velocity projected on the collision unit vector is reflected and rescaled by the restitution coefficient, $(\mathbf{V}' - \mathbf{v}') \cdot \hat{n} = -\alpha(\mathbf{V} - \mathbf{v}) \cdot \hat{n}$, and finally that the kinetic energy $K = \frac{m}{2}|\mathbf{v}|^2 + \frac{I}{2}\omega^2$ changes as

$$K' - K = -\frac{(1 - \alpha^2)}{2} [(\mathbf{V} - \mathbf{v}) \cdot \hat{n}]^2 \frac{m}{1 + \epsilon^2 g^2}. \quad (8)$$

A few relations in cartesian coordinates may be useful: $\mathbf{V} = (-\omega r_y, \omega r_x)$ and $\hat{t} = (-n_y, n_x)$. It is also useful to realize that $\mathbf{V} \cdot \hat{n} = -\omega R_I g$.

Transition rates for a Gaussian gas The transition rate for the collisional Markov process reads [24]

$$W(\omega'|\omega) = \rho S \int \frac{ds}{S} \int d\mathbf{v} \phi(\mathbf{v}) \Theta[(\mathbf{V} - \mathbf{v}) \cdot \hat{n}] \times \quad (9a)$$

$$|(\mathbf{V} - \mathbf{v}) \cdot \hat{n}| \delta[\omega' - \omega - \Delta\omega(s)], \quad (9b)$$

$$\Delta\omega(s) = (1 + \alpha) \frac{[\mathbf{V}(s) - \mathbf{v}] \cdot \hat{n}}{R_I(s)} \frac{g(s)\epsilon^2}{1 + \epsilon^2 g(s)^2}, \quad (9c)$$

where $\phi(\mathbf{v})$ is the pdf for the gas particle velocities and the Heaviside step function $\Theta[(\mathbf{V} - \mathbf{v}) \cdot \hat{n}]$ enforces the kinematic condition necessary for impact.

In our experiments the granular fluid is always quite dilute, with a packing fraction in the range $[2 \div 4\%]$. This is not only sufficient to assume Molecular Chaos, but it has also the positive consequence of producing an almost Gaussian $\phi(\mathbf{v})$, as verified by tracking particles' velocity: $\phi(\mathbf{v}) = \frac{1}{2\pi v_0^2} e^{-\frac{v^2}{2v_0^2}}$, leading to an explicit expression for the transition rates

$$W(\omega'|\omega) = \frac{\rho S R_I^2}{(1 + \alpha)^3 \sqrt{2\pi} \epsilon^2 v_0} \int \frac{ds}{S} |\omega' - \omega| \frac{(1 + \epsilon^2 g^2)^2}{\epsilon^2 g^2} \times \Theta \left[\frac{\omega' - \omega}{g} \right] \exp \left[-\frac{R_I^2}{2\epsilon^2 v_0^2} \left(\omega \epsilon g + \frac{(\omega' - \omega)(1 + \epsilon^2 g^2)}{(1 + \alpha)\epsilon g} \right)^2 \right]. \quad (10)$$

Average velocity in the RCL When $\beta^{-1} \ll 1$ ($\tau_\Delta \ll \tau_c$, denoted as Rare Collisions Limit, RCL), the dynamics is dominated by the rotator at zero velocity with random and independent perturbations due to sparse collisions with gas particles. In this case, the dynamics after each collision event produces an increment of the angular position of the rotator $\Delta\theta$ which depends on the velocity \mathbf{v} of the gas particle, precisely on its projection $v = \mathbf{v} \cdot \hat{n}$, and on the point of impact represented for instance by its curvilinear abscissa s . The formula is

$$\Delta\theta(v, s) = \sigma(\omega_0) \frac{\omega_0^2}{2\Delta} \quad (11)$$

$$\omega_0 = -(1 + \alpha) \frac{v}{R_I} \frac{\epsilon^2 g}{1 + \epsilon^2 g^2}. \quad (12)$$

As a consequence, the average velocity of the ratchet reads

$$\langle \omega \rangle = \frac{\rho S}{2\Delta} \int dv |v| \phi(v) \Theta(-v) \int \frac{ds}{S} \sigma(g) \frac{v^2}{R_I^2} \frac{(1 + \alpha)^2 \epsilon^4 g^2}{(1 + \epsilon^2 g^2)^2} = \frac{\rho S}{\sqrt{2\pi} \Delta} \frac{\epsilon^4 v_0^3}{R_I^2} \left\langle (1 + \alpha)^2 \sigma(g) \frac{g^2}{(1 + \epsilon^2 g^2)^2} \right\rangle_{surf}. \quad (13)$$

where we have used the shorthand notation for the average along the perimeter of the rotator's shape $\langle \rangle_{surf} = \int \frac{ds}{S}$. If one considers the expression for the control parameter β^{-1} we can finally write for the adimensional

angular velocity $\Omega = \frac{R_I}{\epsilon v_0} \omega$

$$\langle \Omega \rangle = \sqrt{\pi} (1 + \alpha)^2 \beta^{-1} \epsilon^2 \left\langle \frac{\sigma(g) g^2}{(1 + \epsilon^2 g^2)^2} \right\rangle_{surf}. \quad (14)$$

Details of the simulations

We have simulated the model described in equations (2) of the Letter, through a suitable adaptation of the Direct Simulation Monte Carlo method (DSMC) [34]. The DSMC is devised to solve numerically a Boltzmann equation, therefore enforcing the Molecular Chaos assumption. In our specific problem, however, the procedure is drastically simplified, since only one particle (the rotator) is represented in the simulation, through its angular velocity and position, ω and θ respectively. The surrounding gas is represented by its constant velocity distribution $\phi(\mathbf{v})$ (assumed Gaussian with variance v_0^2), unaffected by collisions. The dynamics of these variables advances by a series of constant and small time steps of length δt taken smaller than all characteristic time-scales in the problem. At every time step a *free streaming* update and a *collisional* update are performed. The free streaming corresponds to the evolution of ω and θ from t to $t + \delta t$ in the absence of any interrupting collisions. In the *collisional* update, a collision is performed with the probability dictated by the Boltzmann equation (Eq. (3) of the Letter). The correct probability is sampled through a Monte Carlo procedure, where a *tentative* collision is proposed, by choosing the point of impact (at random and uniformly) along the surface of the rotator and by extracting the velocity \mathbf{v} with probability $\phi(\mathbf{v})$. The *tentative* collision is realized with a probability equal to $p_c = (\mathbf{V} - \mathbf{v}) \cdot \hat{n} \rho S \delta t$ (note that δt is chosen much smaller than τ_c and this guarantees that $p_c \ll 1$), leading to an update of ω by the collision rule. Otherwise no collisions occur. Note that the choice of the point of impact (which determines also \hat{n}) can reproduce the precise shape of the experimental rotator (symmetric or chiral).

Control parameter β^{-1} as a good estimate of the ratio of typical times. In Figure 8 we report the ratio between the collision times τ_c and frictional stop times τ_Δ , observed in the simulations in different regimes, in order to assess the fairness of estimate $\beta^{-1} \approx \tau_\Delta / \tau_c$.

-
- [1] T. L. Hill, *Thermodynamics of Small Systems* (Dover Publications, New York, 1964).
 - [2] M. Schliwa and G. Woehlke, *Nature* **422**, 759 (2003).
 - [3] S. Rice *et al.*, *Nature* **402**, 778 (1998).
 - [4] I. Rayment *et al.*, *Science* **261**, 50 (1993).
 - [5] R. Di Leonardo *et al.*, *Proc. Natl. Acad. Sci. USA* **107**, 9541 (2010).

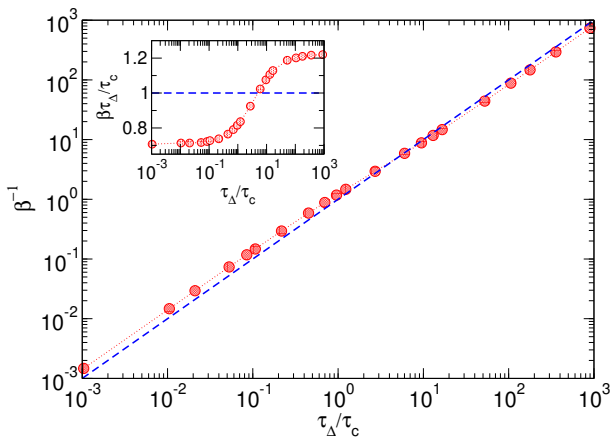


FIG. 8: Assessment of the estimate β^{-1} for τ_{Δ}/τ_c . The ratio between τ_{Δ}/τ_c and β^{-1} obtained in numerical simulations is shown in the inset. The estimate is useful in experiments, where measurements of τ_{Δ} and τ_c are not reliable. It is seen that the estimate is a good approximation of the time-scale ratio where it is close to 1, while it slightly deviates from it in the RCL and FCL, by a factor ~ 1.25 and ~ 0.7 respectively.

- [6] A. Sokolova, M. M. Apodacac, B. A. Grzybowski and I. S. Aranson, Proc. Natl. Acad. Sci. USA **107**, 969 (2010).
- [7] G. Gradenigo, A. Sarracino, D. Villamaina, T. Grigera and A. Puglisi, J. Stat. Mech. L12002 (2010).
- [8] M. v. Smoluchowski M v, Phys. Z. **13**, 1069 (1912).
- [9] R. P. Feynman, R. B. Leighton and M. Sands M, *The Feynman Lectures on Physics* (Addison-Wesley, Reading, MA, 1963), Vol. I, Cap. 46.
- [10] M. M. Magnasco, Phys. Rev. Lett. **71**, 1477 (1993).
- [11] R. D. Astumian, Science **276**, 917 (1997).
- [12] P. Reimann, Phys.Rep. **361**, 57 (2002) .
- [13] P. Hänggi and F. Marchesoni, Rev. Mod. Phys. **81**, 387 (2003).
- [14] H. M. Jaeger, S. R. Nagel, R. P. Behringer, Rev. Mod. Phys. **68**, 1259 (1996).
- [15] G. D'Anna *et al.*, Nature **424**, 909 (2003).
- [16] Z. Farkas, P. Tegzes, A. Vukics and T. Vicsek, Phys. Rev. E **60**, 7022 (1999).
- [17] P. Eshuis, K. van der Weele, D. Lohse and D. van der Meer, Phys. Rev. Lett. **104**, 248001 (2010).
- [18] R. Balzan, F. Dalton, V. Loreto, A. Petri and G. Pontuale, Phys. Rev. E **83**, 031310 (2011).
- [19] G. Costantini, A. Puglisi and U. Marini Bettolo Marconi, Phys. Rev. E **75**, 061124 (2007).
- [20] B. Cleuren B and C. Van den Broeck, Europhys. Lett. **77**, 50003 (2007).
- [21] G. Costantini, U. Marini Bettolo Marconi and A. Puglisi, Europhys. Lett. **82**, 50008 (2008).
- [22] J. Talbot, R. D. Wildman and P. Viot, Phys. Rev. Lett. **107**, 138001 (2011).
- [23] J. Talbot, A. Burdeau and P. Viot, J. Stat. Mech. P03009 (2011).
- [24] B. Cleuren and R. Eichhorn, J. Stat. Mech. P10011 (2008).
- [25] P.-G. de Gennes, J. Stat. Phys. **119**, 953 (2005).
- [26] A. Baule and P. Sollich, Singular features in noise-induced transport with dry friction, Europhys. Lett. **97**, 20001 (2012).
- [27] R. Guerra, U. Tartaglino, A. Vanossi and E. Tosatti, Nature Materials **9**, 634 (2010).
- [28] D. Fleishman, J. Klafter, M. Porto and M. Urbakh, Nano Lett. **7**, 837 (2007).
- [29] A. Naert, Europhys. Lett. **97**, 20010 (2012).
- [30] See Supplemental Material at [URL will be inserted by publisher] for details on experimental setup, theory and simulations.
- [31] R. Bartussek, P. Hänggi and J. G. Kissner, Europhys. Lett. **28**, 459 (1994).
- [32] C. C. de Souza Silva, J. V. de Vondel, M. Morelle and V. Moshchalkov, Nature **440**, 651 (2006).
- [33] J. E. Villegas *et al.*, Science **302**, 1188 (2003).
- [34] G. A. Bird *Molecular Gas Dynamics and the Direct Simulation of Gas Flows* (Clarendon, Oxford, 1994).
- [35] G. Gradenigo, A. Sarracino, D. Villamaina and A. Puglisi, Europhys. Lett. **96**, 14004 (2011) and A. Sarracino, D. Villamaina, G. Gradenigo, A. Puglisi, Europhys. Lett. **92**, 34001 (2010).
- [36] A. Puglisi, A. Gnoli, G. Gradenigo, A. Sarracino and D. Villamaina, J. Chem. Phys. **136**, 014704 (2012).